Title:	Punching shear tests on compact footings with uniform soil pressure
Authors:	Simões J. T., Bujnak J., Fernández Ruiz M., Muttoni A.
Published in:	Structural Concrete http://onlinelibrary.wiley.com/doi/10.1002/suco.201500175/abstract
DOI	10.1002/suco.201500175
Volume: Pages:	n° 4 pp. 603-617
Country:	Suisse
Year of publication:	2016
Type of publication:	Peer reviewed journal article

Please quote as:	Simões J. T., Bujnak J., Fernández Ruiz M., Muttoni A., *Punching shear tests on compact footings with uniform soil pressure*, Structural Concrete, n° 4, Suisse, 2016, pp. 603-617.

João T. Simões*
Jan Bujnak
Miguel Fernández Ruiz
Aurelio Muttoni

Punching shear tests on compact footings with uniform soil pressure

Punching shear is usually the governing failure criterion when selecting the depth of reinforced concrete footings. Despite the fact that large experimental programmes aimed at the punching strength of slender flat slabs have been performed in the past, only a few experimental campaigns on full-scale compact reinforced concrete footings can be found in the literature. This paper presents the results of an experimental programme including eight reinforced concrete footings with a nominal thickness of 550 mm. These experiments investigated the influence of column size, member slenderness and the presence of compression and shear reinforcement. The tests were performed using an innovative test setup to ensure a uniform soil pressure. The experimental results show that slenderness influences the punching shear strength as well as the effectiveness of the shear reinforcement. The experiments also show that an important interaction occurs between bending and shear for high levels of shear force near the column (the typical case of compact footings or members with large amounts of shear reinforcement). Different continuous measurements recorded during the experimental tests allow a complete description of the kinematics and strains at failure. On that basis, experimental evidence is obtained showing that crushing of the concrete struts near the column is the phenomenon that triggers the punching failure of compact footings.

1 Introduction

Several experimental investigations regarding the punching shear behaviour of reinforced concrete footings have been performed in the past [1]–[18]. They can be classified on the basis of the test setup, where four types can be distinguished. The first test setup refers to the cases where the footings were supported on a bed of springs and were loaded through a column stub [1], [2] (see to Fig. 1a). This arrangement may reproduce actual conditions for perfectly elastic soils, but the analysis of the results due to the non-uniform distribution of the reaction pressure (which

* Corresponding author: joao.simoes@epfl.ch

depends on the deformations of the footings and varies during the test) is not straightforward. A second configuration often used consists of footings resting on line or concentrated supports, with the load being applied by a column stub or steel plate, see Fig. 1b [6], [7], [15]–[17]. A similar configuration, which is considered to be part of the same group, is the application of a finite number of concentrated loads at a certain distance from the column, which is fixed to a reaction frame. This configuration therefore presents two slightly different options: i) equal displacements and ii) equal force at the line of supports or concentrated loads. Although useful information for analysing the influence of different geometrical and mechanical properties can be obtained from this type of experimental test, both the inclination of the compression struts and the punching failure surface are geometrically defined by the test setup (the latter developing between the edge of the column and the inner radius of the supports). Therefore, in most of the tests on footings subjected to concentrated loads, the failure surface might not have developed in a completely free manner, instead being defined geometrically by the load arrangement.

As shown schematically in Fig. 1c, another test setup configuration currently used consists of applying an effective uniform loading replicated through the use of several load points [3]–[5], [8]–[14]. These load points are supposed to represent the resultant of a uniform pressure in each sub-area. It should nevertheless be noted that if the distance between load points becomes large, these tests might also lead to a geometrical definition of the failure surface. In fact, this is an important issue when testing full-scale specimens with this configuration, since a finite number of load points has to be applied over a large surface. Recently, a more realistic configuration has been used [8]–[12], consisting of footings supported on sand and loaded through the column (see Fig. 1d). The failure surface can develop freely in this configuration, but – similarly to the situation in the test configuration with footings supported on a bed of springs – soil pressure concentrations can occur. In addition, soil behaviour may be difficult to characterize and pressure measurements are needed in order to know the exact distribution of the soil reaction. Nevertheless, these tests represent a valuable experimental contribution, allowing the investigation of the soil-structure interaction.
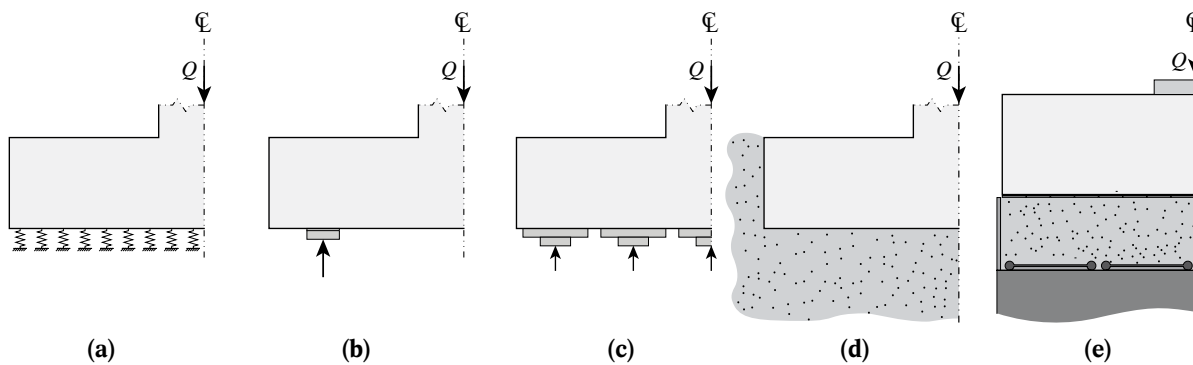
Fig. 1. Typical test setup configurations used in experimental investigations of the punching shear strength of footings

For the reasons discussed previously, few experimental full-scale tests under complete uniform soil pressure are available and more data is still needed. An experimental investigation of eight full-scale reinforced concrete footings with an innovative test setup is presented in this paper (Fig. 1e). This setup enables the application of a uniform soil pressure to the bottom surface of the specimens. For that purpose, a group of flat jacks connected in series (equal pressure) was placed in the bottom of a rigid box, which was then filled with a layer of sand ~300 mm deep, thus ensuring a uniform distribution of the load and, consequently, the application of a uniform soil pressure. A sheet of polytetrafluoroethylene (PTFE) and small aluminium plates were also placed between the footings and the layer of sand to reduce the friction between soil and footing. Some parameters were kept constant – nominal bottom flexural reinforcement ratio (0.75 %), nominal concrete compressive strength (30 MPa) and nominal thickness (550 mm) – and others varied. The parameters whose influence was investigated were: column size, footing side length (allowing variations in shear slenderness), the presence of shear reinforcement and the presence of horizontal reinforcement in the theoretical compression zone. With respect to the shear slenderness, in this paper it will be defined as the ratio between the clear shear span and the effective depth, where the effective clear shear span is defined as the distance between the edge of the footing and the edge of the column measured in the principal directions of the reinforcement (placed orthogonally).

Every test was tracked with several continuous measurements to allow an understanding of the kinematics and strains in the specimen. Four different behaviour regimes could be clearly distinguished and they are described in this paper.

2 Experimental programme
2.1 Specimens and materials

The footings were square with a side length of 2.12 m (PS11, PS12, PP7, PP8) or 1.59 m (PS13, PS14, PS15, PP9). The columns used were also square with a side length of 0.30 m (PS11, PS13, PS14, PS15, PP7, PP9) or 0.45 m (PS12, PP8).The bottom flexural reinforcement was arranged orthogonally and its nominal reinforcement ratio was kept constant for all eight specimens (ratio of 0.75 %, 22 mm diameter bars at a constant spacing of

100 mm, see Fig. 2). Horizontal reinforcement in the top face (theoretical compression surface) was also used, but only for some specimens (footings PS14 and PS15 had no top reinforcement). When provided, the compression reinforcement was kept constant (with a ratio of 0.39 %, consisting of 16 mm diameter bars at a constant spacing of 100 mm). Both bottom and top reinforcement was bent near the edges (Fig. 2). The nominal cover was 20 mm.

Footings PP7, PP8, PP9 and PS15 had shear reinforcement consisting of 25 mm diameter double-headed shear studs in a radial arrangement. The layout of the shear reinforcement for each footing is presented in Fig. 3: PP7 had three perimeters with 16 studs, PP8 three perimeters with 20 studs and PP9 and PS15 two perimeters with 16 studs. In order to ensure the correct positions of the studs, steel strips (800 × 30 × 4 mm for PP7 and PP8, and 550 × 30 × 4 mm for PP9 and PS15) were welded to the heads of the studs and the position of the flexural reinforcement was adjusted slightly where necessary.

The concrete used in all footings was of normal strength (nominal concrete compressive strength of 30 MPa) with a maximum aggregate size of 16 mm. Concrete cylinders (320 mm high, 160 mm diameter) were cast, tested and used to verify the concrete strength. Ordinary reinforcing steel with a characteristic yield strength of 500 MPa was used in all the footings for both flexural and shear reinforcement. Its corresponding mechanical properties were measured on three different samples of each different diameter. The cylinder concrete compressive strength on the day of the punching tests and the yield strength of the reinforcement for each specimen can be found in Table 1.

2.2 Test setup and experimental procedure

The test setup is shown in Fig. 4. It consisted of a loading system under the footing and a reaction frame above it (also used as a loading system in some cases). The loading system under the footing consisted of a box containing a group of flat jacks hydraulically connected with a copper tube (16 jacks for the larger specimens, nine for the smaller ones). The flat jacks were square with a side length of 500 mm and a nominal height of 55 mm. An electric pump was used to introduce water into the group of flat jacks to inflate them. The application of a uniform pressure to the bottom surface of the footing was ensured through the introduction of a layer of sand between it and
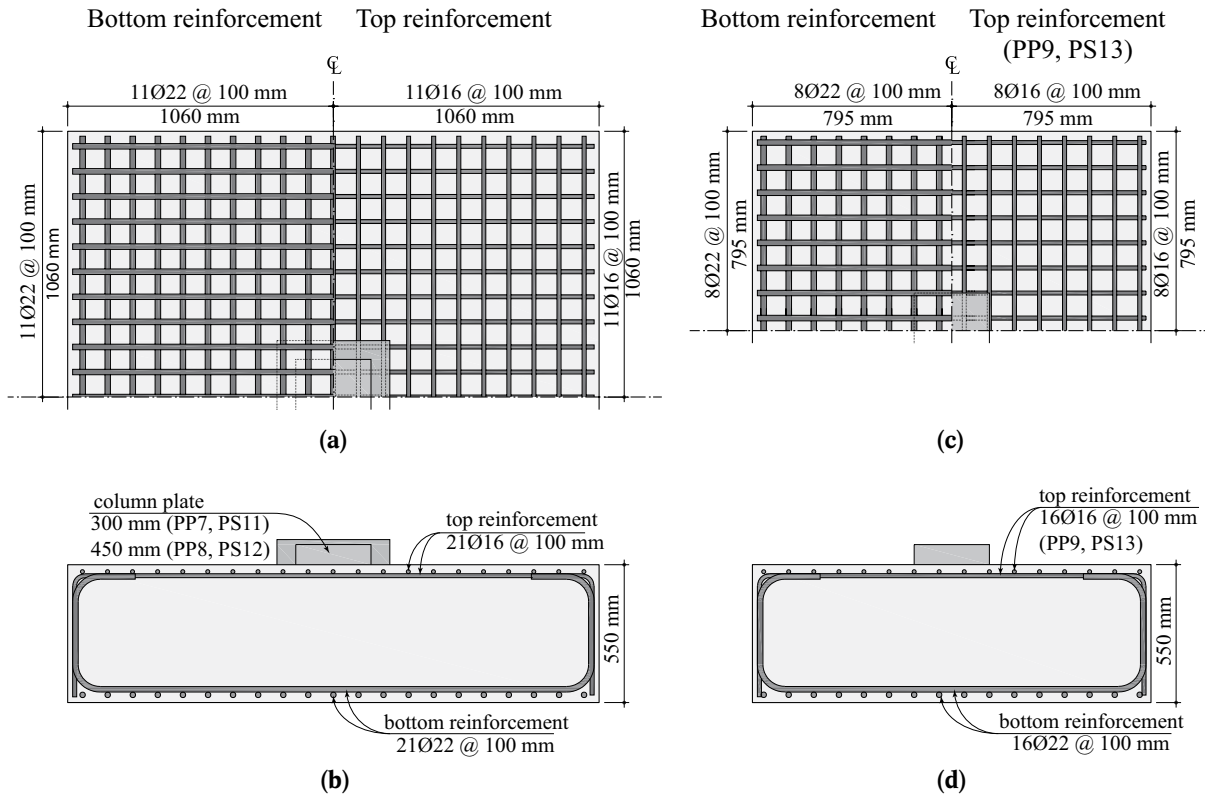
Bottom reinforcement   Top reinforcement

11Ø22 @ 100 mm   11Ø16 @ 100 mm
1060 mm   1060 mm

11Ø22 @ 100 mm
1060 mm

11Ø16 @ 100 mm
1060 mm

(a)

Bottom reinforcement   Top reinforcement
(PP9, PS13)

8Ø22 @ 100 mm   8Ø16 @ 100 mm
795 mm   795 mm

8Ø22 @ 100 mm
795 mm

8Ø16 @ 100 mm
795 mm

(c)

column plate
300 mm (PP7, PS11)
450 mm (PP8, PS12)

top reinforcement
21Ø16 @ 100 mm

550 mm

bottom reinforcement
21Ø22 @ 100 mm

(b)

top reinforcement
16Ø16 @ 100 mm
(PP9, PS13)

550 mm

bottom reinforcement
16Ø22 @ 100 mm

(d)

Fig. 2. Plan and section view of layout of flexural reinforcement: a) and b) PS11, PS12, PP7, PP8; c) and d) PS13, PS14, PS15 and PP9

Ø25 double-headed studs
3 stud perimeters
16 studs per perimeter

Ø25 double-headed studs
3 stud perimeters
20 studs per perimeter

PP7   PP8

Ø25 double-headed studs
2 stud perimeters
16 studs per perimeter

Ø25 double-headed studs
2 stud perimeters
16 studs per perimeter

PP9   PS15

(a)   **(b)**

PP7   PP8

75   75

508   25
250   250   150

25
150   250   250
508

550

PP9   PS15

75   75

508   25
250   150

25
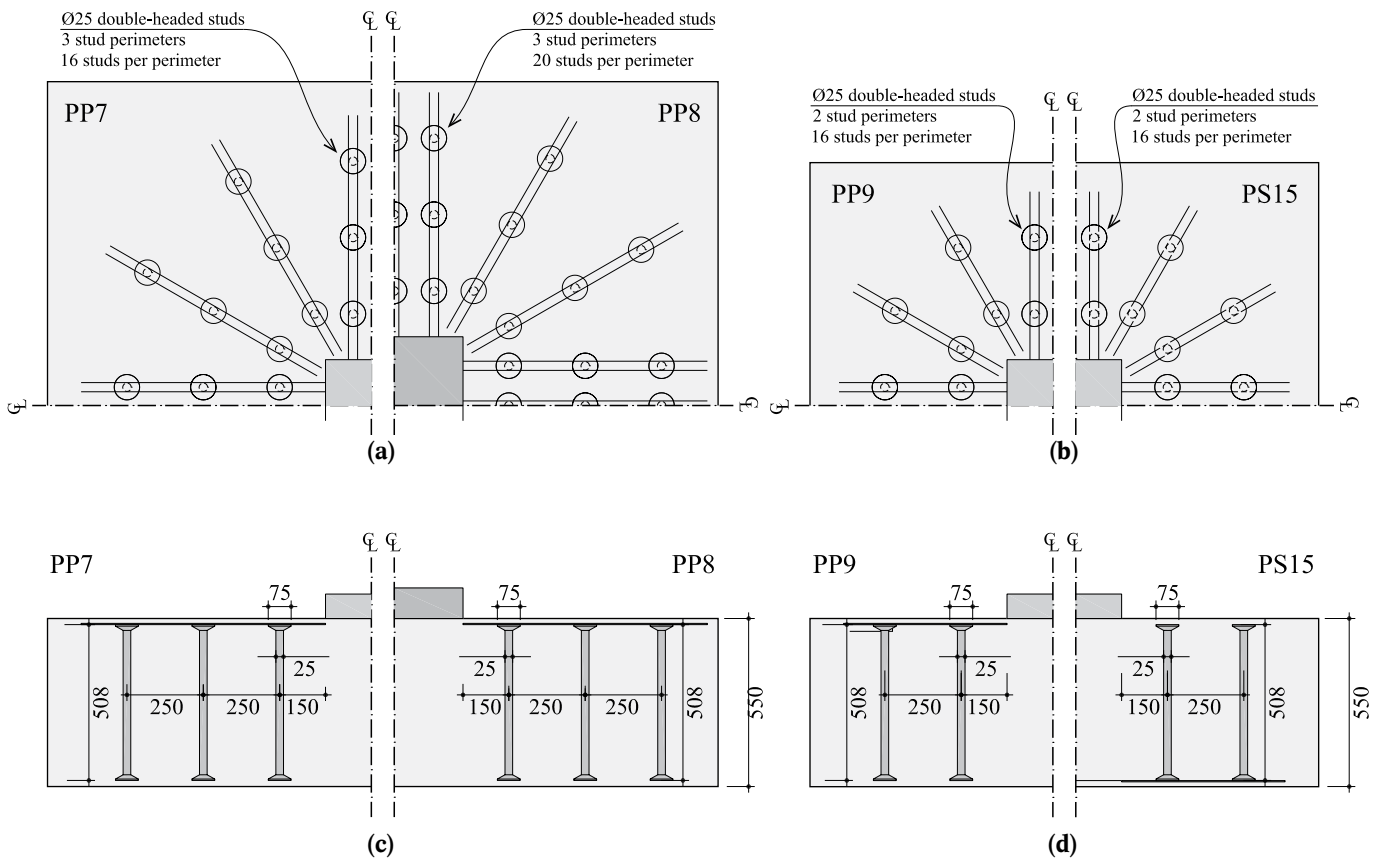150   250
508

550

(c)   **(d)**

Fig. 3. Layout of shear reinforcement: a) plan of PP7 and PP8, b) plan of PP9 and PS15, c)section through PP7 and PP8, and d) section through PP9 and PS15

Table 1. Main properties of experimental investigation

Specimen	B [mm]	c [mm]	d [mm]	a/d [–]	c/d [–]	ρ [%]	f_y [MPa]	f_c [MPa]	n_s	n_p	ϕ_w [mm]	f_{yw} [MPa]
PS11	2.12	0.30	0.509	1.79	0.59	0.740	517	29.5	–	–	–	–
PS12	2.12	0.45	0.512	1.63	0.88	0.735	517	31.1	–	–	–	–
PS13	1.59	0.30	0.506	1.27	0.59	0.756	517	32.1	–	–	–	–
PS14	1.59	0.30	0.510	1.26	0.59	0.750	537	31.9	–	–	–	–
PP7	2.12	0.30	0.497	1.83	0.60	0.758	580	33.7	16	3	25	567
PP8[1]	2.12	0.45	0.510	1.64	0.88	0.738	580	34.5	20	3	25	567
PP9	1.59	0.30	0.516	1.25	0.58	0.741	580	34.8	16	2	25	567
PS15	1.59	0.30	0.511	1.26	0.59	0.749	537	32.2	16	2	25	578

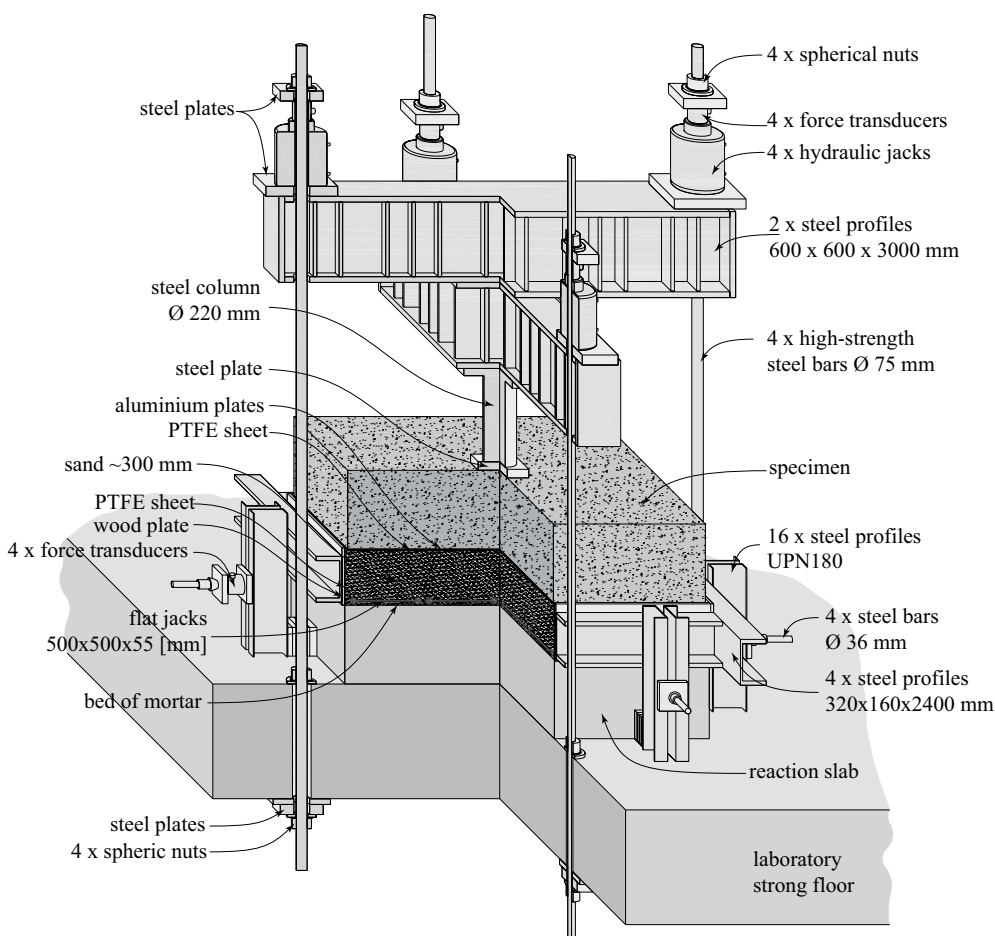[1] Experimental test stopped due to large deformations

Fig. 4. Schematic representation of test setup

the flat jacks (compensating for the gaps between their effective areas). The sand was confined laterally by the faces of a box made from four steel channel sections. A sheet of PTFE was placed between the sand and the lateral surfaces of the box, thus avoiding that the uplift of the sand would be constrained by friction. A gap of approx. 20 mm was additionally left between the lateral surfaces of the footing and the lateral surfaces of the box to allow expansion of the bottom surface of the footing. In order to reduce friction between the sand and the specimen, a sheet of PTFE and aluminium plates ($130 \times 130 \times 5$ mm) were placed between them.

The reaction frame above the footing consisted of two perpendicular steel beams connected to a high-strength steel column. The two steel beams were fixed to the strong floor of the laboratory with four high-strength $\varnothing$ 75 mm threaded bars. The column was simulated by a square steel plate placed between the footing and the high-strength steel column. A thin layer of plaster was placed between the steel column plate and the specimens in order to avoid any local stress concentrations.

For specimens PP7 and PP8, the entire load was applied through the loading system under the footing. For the remaining tests, four hydraulic jacks were placed on
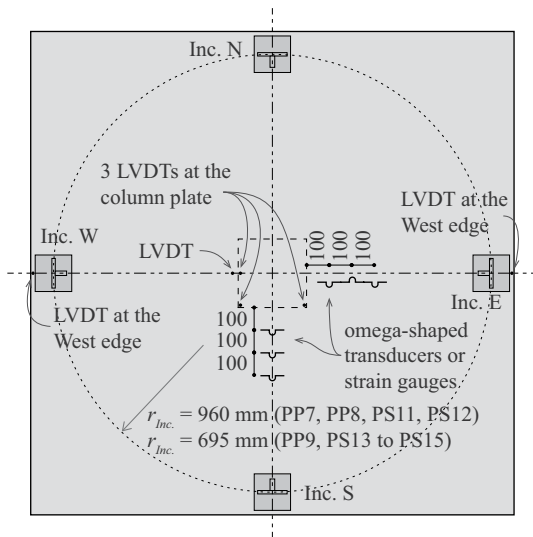
Fig. 5. Schematic representation of the main measurement devices and their locations

top of the reaction frame. These jacks were used to apply part of the load at the beginning of the test, thus reducing the necessary deformation of the flat jacks.

With respect to the experimental procedure, a loading rate of 50 kN/min was applied. Load steps were used during the loading of specimens PP7 to PP9 and PS11 to PS13 to perform measurements whose results are beyond the scope of this paper.

2.3 Measurement devices

A general overview of the main measurement devices is shown in Fig. 5. The applied force was measured with four load cells placed on top of the reaction frame, four strain gauges placed on the steel column with the oil pressure measured in the hydraulic jacks (placed on the top of the reaction frame) and with the water pressure measured in the flat jacks under the sand bed. Negligible differences were observed between the different devices. The footing rotation was measured on the top surface of the footing with four inclinometers aligned with the axis and placed 100 mm from the edge of the footing. The strains at the concrete top surface were measured in radial and tangential directions with the help of three omega-shaped gauges

(PP7 to PP9, PS11 to PS13) or strain gauges (PP14 and PS15) with a base length of 100 mm. Vertical displacements were also measured at different locations on the top surface with linear variable differential transformers (LVDT), notably at the edges of the footing aligned with the axis. Three LVDTs were also placed on the steel column plate, enabling the calculation of the vertical displacement at its centre. The changes in the thickness of the footing were also measured in specimens PS11 to PS15 at different distances from the column edge. The strains in the bottom flexural reinforcement of specimen PS12 were measured at different locations using strain gauges with a base length of 6 mm. Deformations of double-headed shear studs were measured using the same strain gauges. The expansion of the top and south lateral surfaces of specimens PS14 and PS15 was measured with LVDTs, as will be described later.

3 Experimental results
3.1 Main results

The main results of the experimental campaign are presented in Table 2. After testing, cracking was observed on the bottom surface, regularly spaced and coincident with the location of the reinforcing bars in both directions (see, for instance, Fig. 6). To investigate the tangential cracking and punching cone, the specimens were sawn along (at least) the weak axis (axis with smaller effective depth of reinforcement). The cracking patterns observed are presented in Fig. 7 (where the punching cone can be clearly seen). The specimens with shear reinforcement (PP7, PP9 and PS15) failed in punching inside the shear-reinforced zone by crushing of the concrete struts near the loading plate. The test on specimen PP8 with shear reinforcement was stopped after large plastic deformations. Nevertheless, shear cracks can be very clearly seen, indicating that a punching failure was probably about to occur.

On the basis of the saw-cuts (Fig. 7), failure can be associated with the crushing observed along the failure surface, notably, close to the column (where various parallel cracks appear). The specimens with shear reinforcement exhibited a more ductile failure than those without shear reinforcement. With the exception of specimen PP8, every footing with transverse reinforcement presented a clear crushing failure characterized by the development of

Table 2. Results of experimental investigation

Specimen	Q_R [MN]	Q_{flex} [MN]	Q_R/Q_{flex}	$Q_R/d^2f_c^{1/2}$ [MPa$^{1/2}$]	$Q_{R,\,with}/Q_{R,\,without}$
PS11	4.769	10.059	0.474	3.389	
PS12	6.839	12.065	0.567	4.678	
PS13	6.285	11.422	0.550	4.333	–
PS14	5.896	11.421	0.516	4.013	
PP7	7.651	11.014	0.695	5.336	1.57
PP8	10.868[1]	13.469	0.807[1]	7.114[1]	1.52[1]
PP9	9.020	13.054	0.691	5.743	1.33
PS15	8.260	11.363	0.727	5.575	1.39

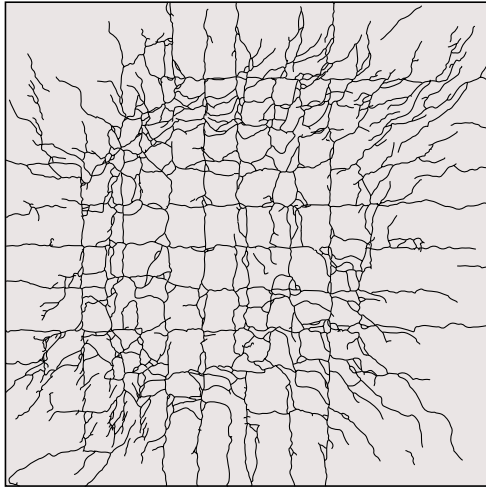[1] Experimental test stopped due to large deformations

Fig. 6. Schematic representation of cracking pattern on bottom surface of specimen PS14 after testing

a failure surface between the edge of the column and the first row perimeter of studs.

It is also important to note from Fig. 7 that the inclination of the failure surface of footings without shear reinforcement appears to be dependent on the shear slenderness, with steeper surfaces observed for more compact slabs. This is in agreement with previous experimental campaigns presented in the literature [11]–[14].

3.2 Measured deformations
3.2.1 Rotation and deflections

The load–rotation curves of the test specimens are presented in Fig. 8, where the specimens without shear rein-

forcement are compared with the corresponding shear-reinforced specimens. From that figure it can be observed that the presence of shear reinforcement enhances the strength and the deformation capacity. Both footings with and without shear reinforcement experienced a decrease in the tangent flexural stiffness. For specimens without transverse reinforcement, this was observed close to the failure load, whereas for specimens with shear reinforcement, this decrease was observed at lower load levels (see Fig. 8).

Figs. 9a–9d show the load–displacement curves obtained using different measurement devices for three specimens without shear reinforcement (PS11 to PS13) and for one specimen with shear reinforcement (PS15). The displacements presented in this figure were calculated based on the rotations measured with four inclinometers and on the displacement measured with LVDTs at the column plate or edge (Fig. 9e). Three different components can be distinguished, corresponding to flexural deformations δ_ψ, shear deformations δ_γ and, finally, column penetration δ_p, as shown in Fig. 9e. It is important to note that the information shown in Fig. 9 is calculated based on the measured deformations at the top surface of the specimens. It is also important to note that part of the deformation, considered here as column penetration, may also be considered as a shear deformation (here it will be separated for clarity). In this respect, it can be seen that the punching failures of the footings without shear reinforcement presented an enhanced total deformation capacity (sum of flexural, shear and column penetration) with respect to slender flat slabs [22] (where the flexural deformation component is dominant).

The three specimens without shear reinforcement shown in Figs. 8a–8c differ in the span-to-effective depth
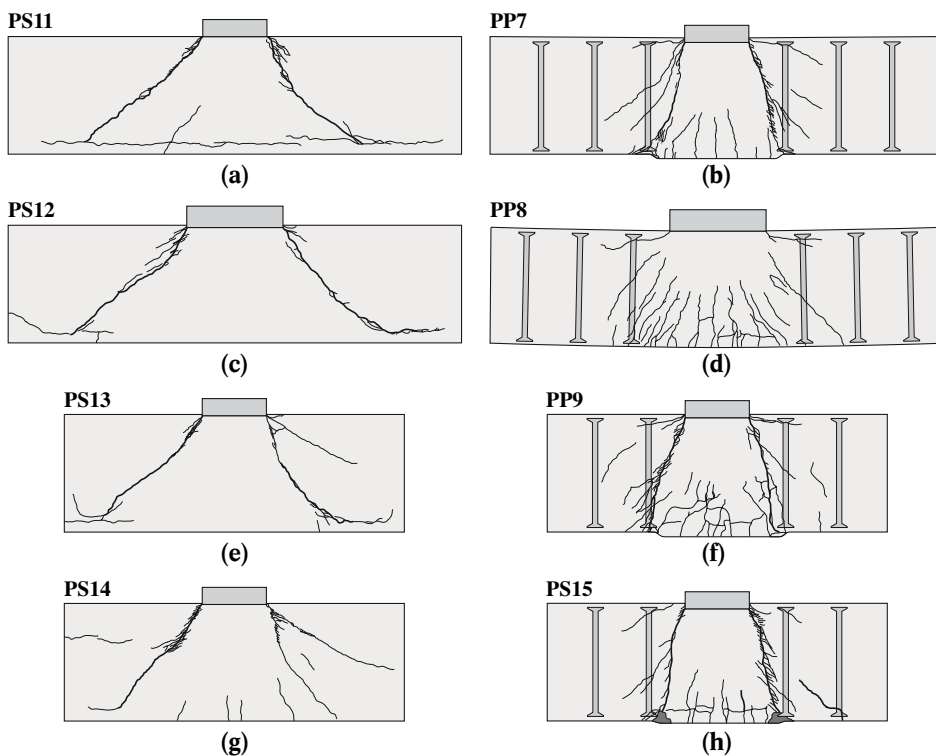

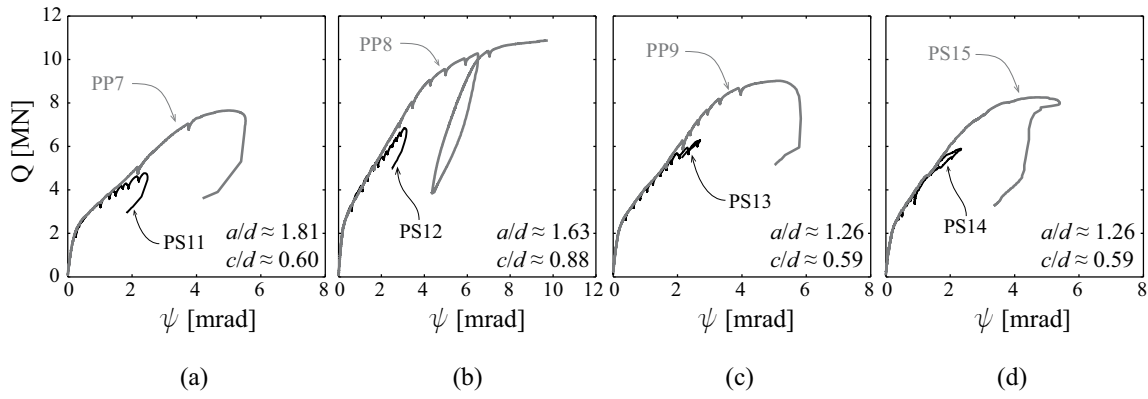**Fig. 7.** Schematic representations of the saw-cuts

Fig. 8. Load-rotation curves of the corresponding specimens with and without shear reinforcement
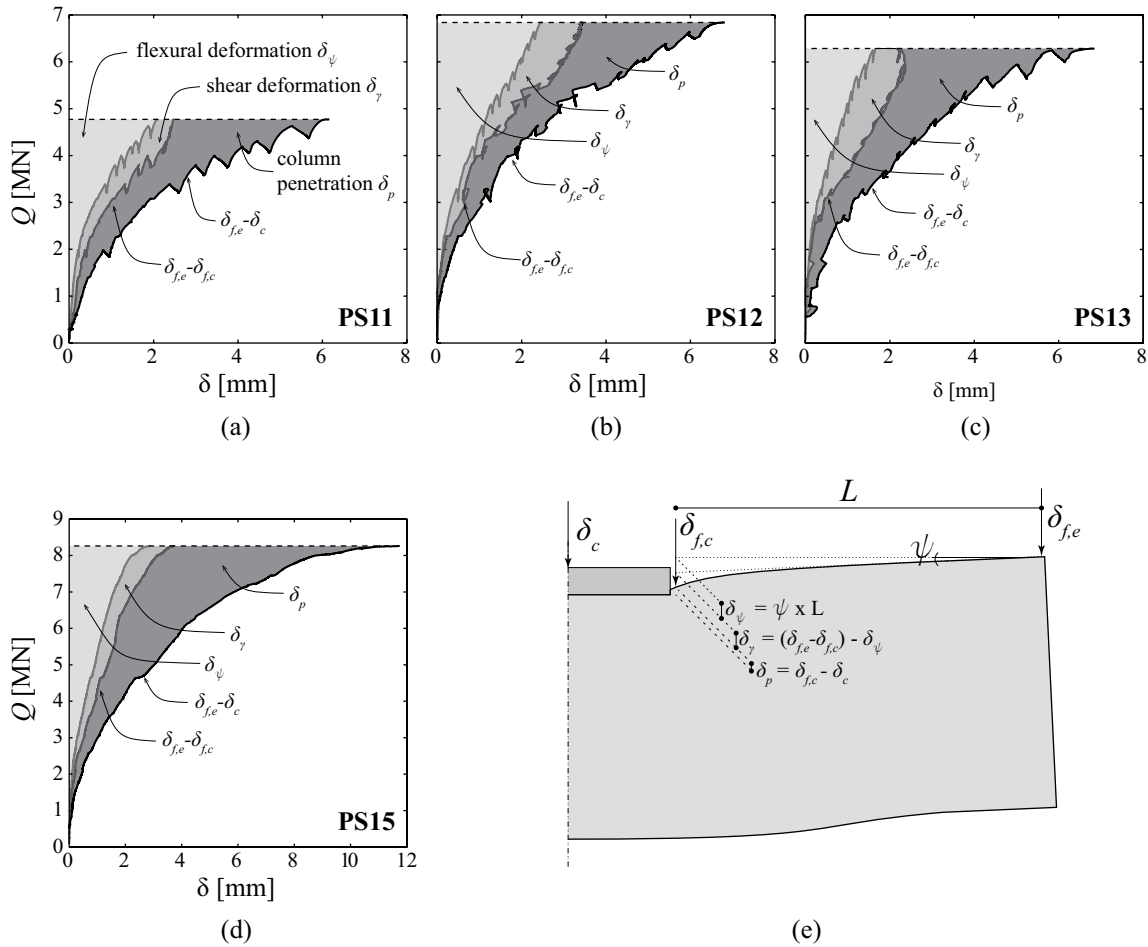

Fig. 9. Load-displacement curves showing, separately, the flexural deformation (estimated based on the rotation of the footing), shear deformation and column penetration of: a) PS11, b) PS12, c) PS13, d) PS15, and e) scheme of recorded measurements: outer rotation ψ by inclinometers, vertical displacement at edge of footing $\delta_{f,e}$ with an LVDT, vertical displacement of footing 25 mm from column edge $\delta_{f,c}$ and vertical displacement at centre of column plate δ_c.

ratio and the column size. For all specimens, the sum of the shear deformation and column penetration can be of the same, or even higher, magnitude than the flexural deformations. It is also possible to verify that the column penetration, which can be seen as a very local deformation, can reach non-negligible values, particularly for the most compact footings, as a result of high levels of shear force. It is interesting to note that for the smallest column size, the shear deformation stabilized or even decreased near failure. This result is explained by the fact that a part of the shear deformation is accounted for as a column penetration.

Based on the measurements recorded, the deformed shape of the footing during loading can be drawn as shown in Fig. 9e, where the three components (flexural and shear deformations plus column penetration) are taken into account qualitatively. Fig. 9d refers to footing PS15, which corresponds to a shear-reinforced footing without horizontal top reinforcement. In the case of shear-reinforced specimens, the three deformation components can again be clearly distinguished. Although an increase in flexural deformations is observed close to failure in the case of the shear-reinforced specimen (a plateau seems to be reached in the load–rotation curves, see
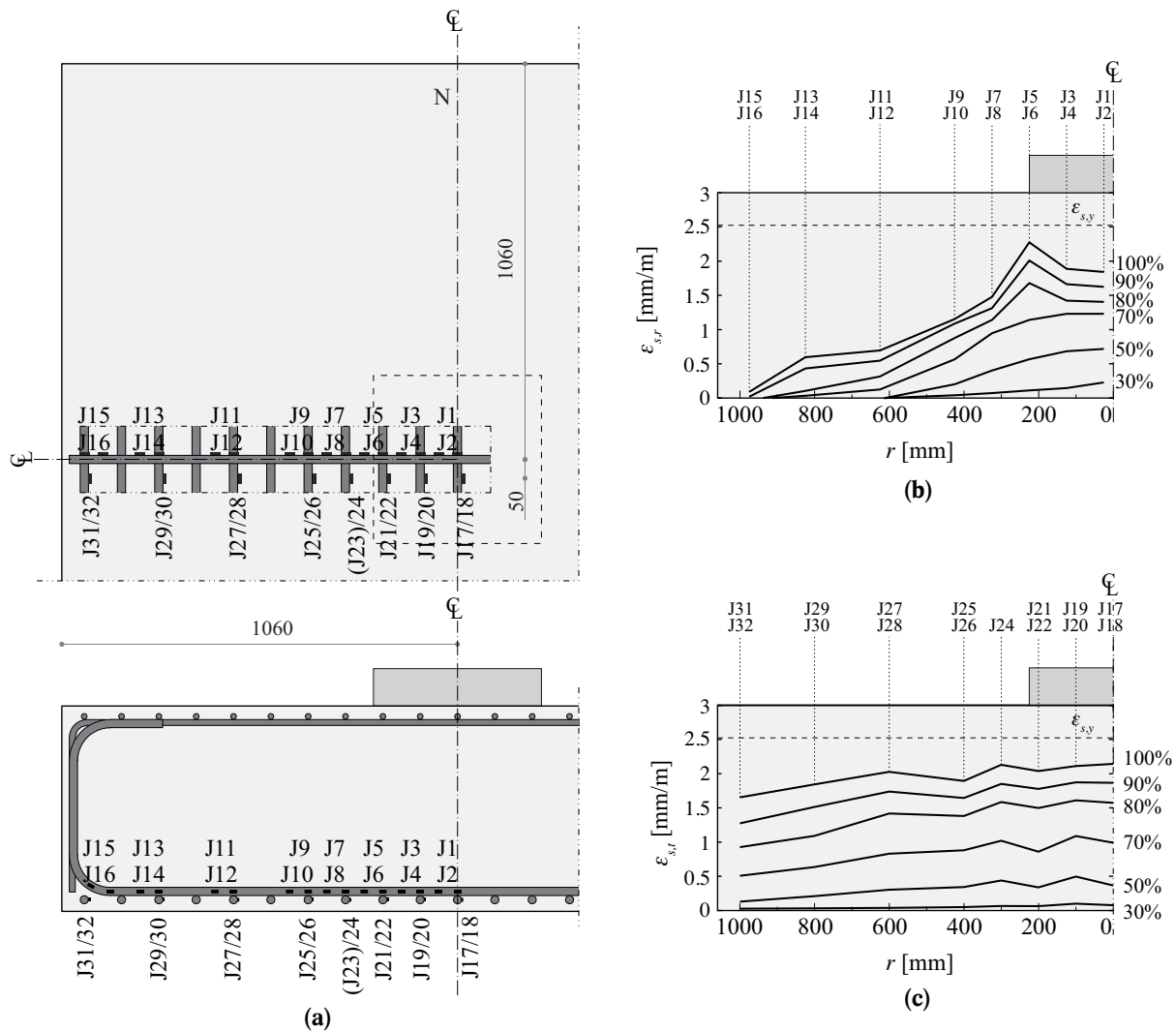
Fig. 10. Strains in the bottom flexural reinforcement of specimen PS12: a) location of the 32 strain gauges used (16 in radial and 16 in tangential direction along the axis in the weak direction), b) radial strains J1–J16, and c) tangential strains J17–J32 (J23 not considered) (percentages indicate load level compared with maximum load).

Fig. 8d), a more significant increase in the column penetration is again observed.

3.2.2 Strains in bottom flexural reinforcement

The strains in the bottom flexural reinforcement of specimen PS12 were tracked along the weak axis in both the radial and tangential directions. The location of the 32 strain gauges is shown in Fig. 10a (where strain gauge J23 is not considered here in after due to measurement problems during the test). Although the specimen is square and not circular, strain gauges J17 to J32 can be considered as indicators of tangential strains. The results are presented in Figs. 10b and 10c for radial and tangential directions respectively. Each value represented in these two figures results from the average value of two strain gauges placed at a distance of 50 mm, e.g. $\varepsilon_{s,r}$ at $r = 5$ mm is the average of J1 ($r = 0$ mm) and ($r = 50$ mm), where r is the radial distance from the centre of the specimen. It is interesting to note that a peak on the strains profile develops at the edge of the column in the radial direction (although the average value at this position is below the yielding strain, the strain gauge placed at $r = 250$ mm reached the yielding

strain locally). It should also be noted that the tangential strains measured near the edge of the footing are larger than those measured in the radial direction.

3.2.3 Changes in the thickness of the footings

The changes in the thickness of the specimens were measured at different points in specimens without shear reinforcement and also in the shear-reinforced footing PS15 (measurement details are shown in Fig. 11a). The results are presented in Fig. 11, where it remains clear that the variation in the thickness at maximum load tends to be more pronounced for the most compact footings (see Figs. 11b–11e). It should be noted that the changes in thickness measured correspond to the vertical component of shear cracks developing inside the footing. It is possible to verify that the changes in the thickness of the footings start to be significant at values of ~80 % of the maximum load for the specimens without shear reinforcement. It is also interesting to note that changes in thickness tend to be more pronounced near the column. With respect to the shear-reinforced specimen (Fig. 11f), it was shown that the changes in the thickness variation start at ~60 % of the
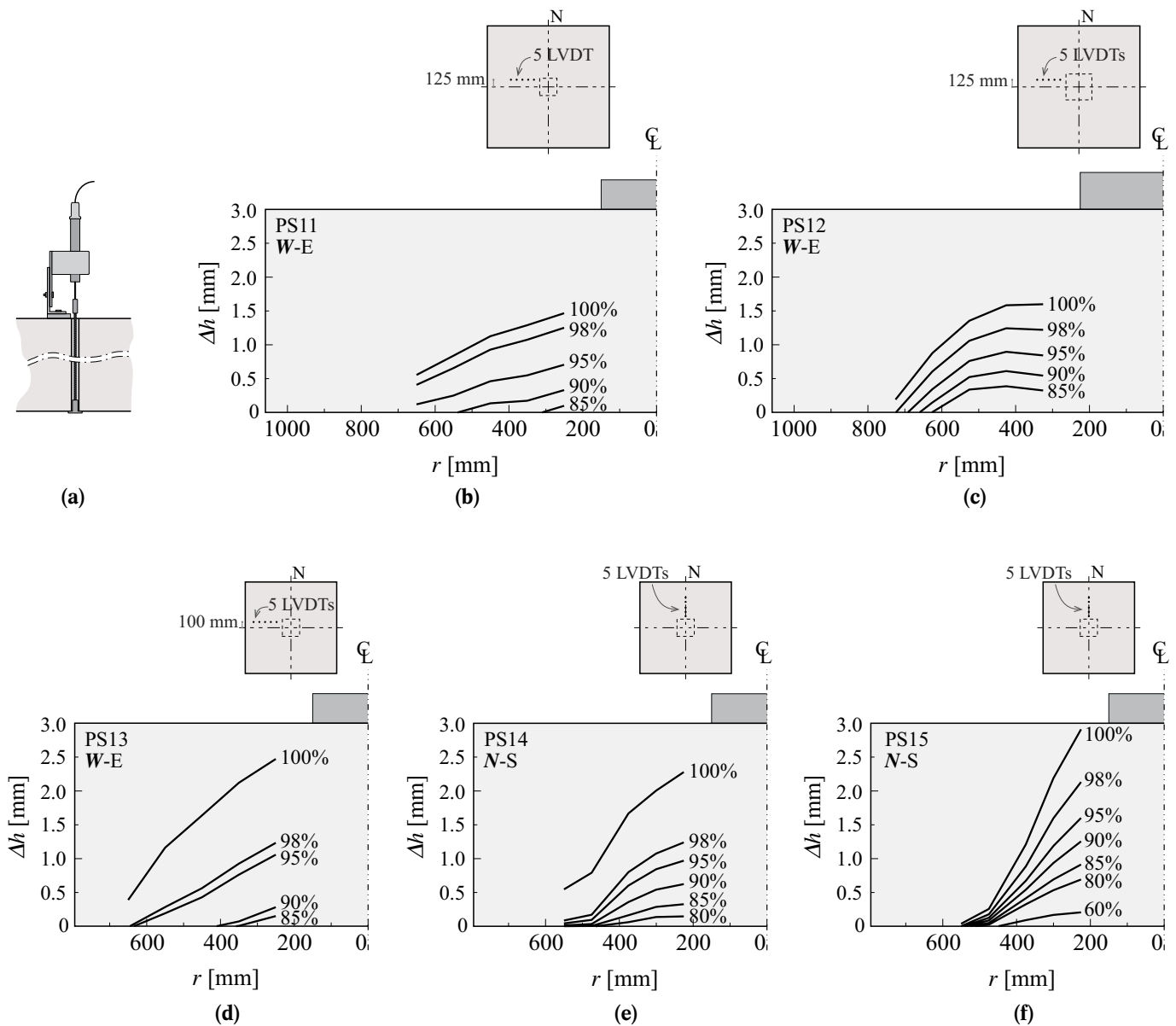
Fig. 11. Changes in thickness for different load levels and locations of measuring points: a) detail of measurement device; b) PS11,c) PS12,d) PS13,e) PS14,f) PS15 (percentages indicate load level compared with maximum load).

maximum load, which corresponds to the load at which the changes in the thickness of the reference specimen – without shear reinforcement – can also be observed.

3.2.4 Strains at the concrete top surface

The strains at the concrete top surface were measured near the column plate. The radial and tangential strains measured for specimen PS11 (most slender specimen) are shown in Figs. 12a and 12b respectively. With respect to radial strains, an elongation was measured, with higher values obtained for smaller distances from the column plate. This elongation increases with increasing levels of load up to ~80 % of the total load, after which it starts decreasing. At failure, values of radial strain at the concrete top surface near the column are very small. This behaviour, which was measured consistently during this experimental campaign, has already been observed in footings in previous experimental investigations (e.g. [4], [5], [8]–[14]). This behaviour is very different from that normally ob-

served in flat slender slabs (e.g. [19]–[22]), where a shortening (related to compression) was measured in the soffit of the slab up to a certain value, after which a decompression was normally observed. With respect to the tangential strains at the concrete top surface, it should be noted that a shortening (related to compression) proportional to the rotation (as a result of flexural deformations) was measured up to a certain value, where a tendency towards stabilization or even a slight decrease in the tangential strains could be measured consistently.

3.3 Global observed behaviour of RC footings subjected to concentrated loads

The punching shear strength of the specimens with shear reinforcement is normally governed by one of the three following failures modes: crushing of the concrete struts between the column and the first perimeter of shear reinforcement, a failure within or outside the shear-reinforced area [23]. The shear-reinforced specimens in this paper
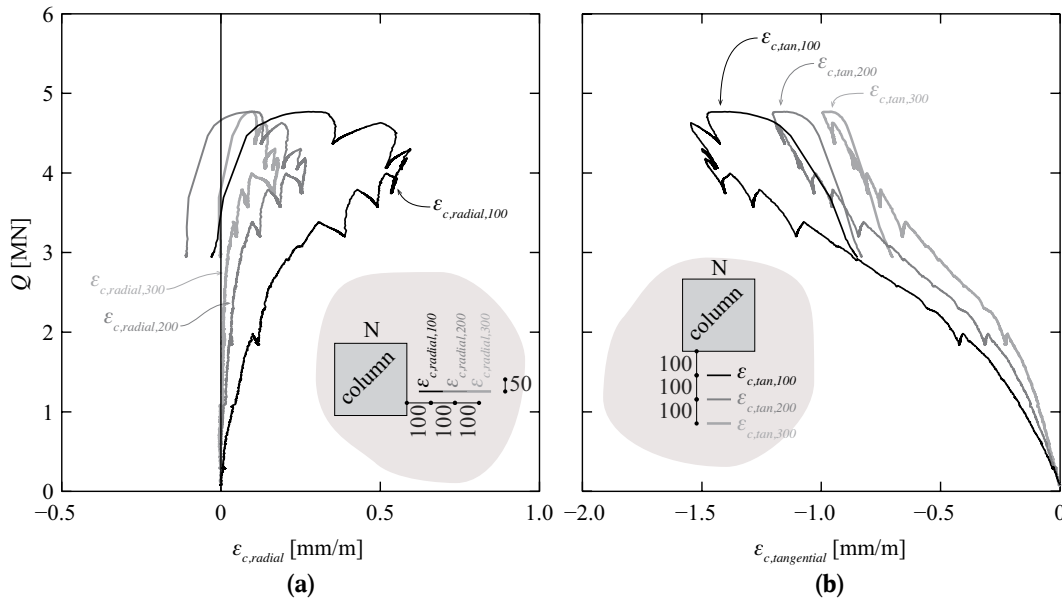
Fig. 12. Strains at the concrete top surface of test PS11 in a) radial and b) tangential directions (positive values indicate elongation)
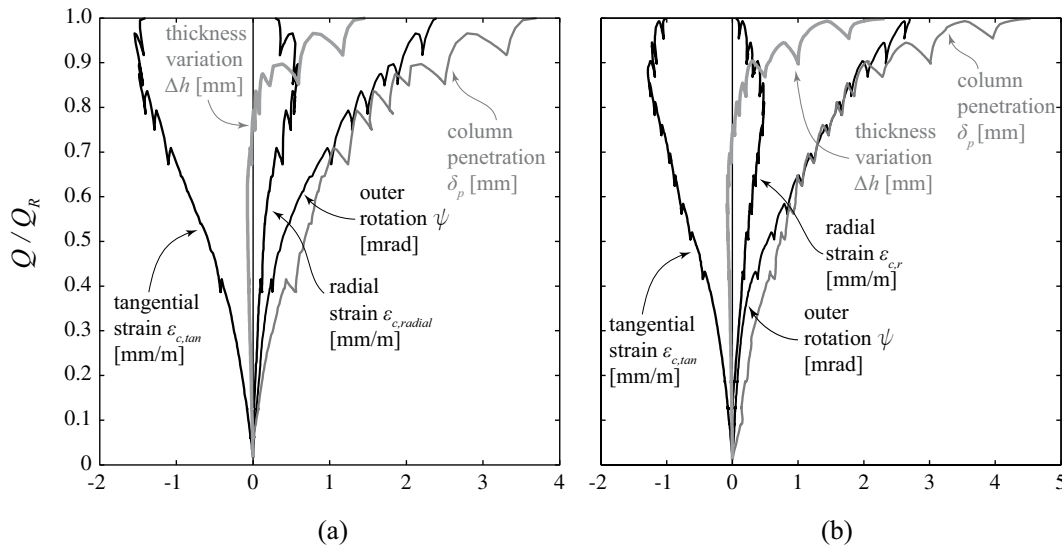

Fig. 13. Representation of different deformations recorded in the shear-critical region for footings: a) PS11, b) PS13; rotation measured at the concrete top surface, column penetration, thickness variation measured 100 mm from edge of column plate, radial and tangential strains at the concrete top surface measured 100 mm from edge of column plate with omega-shaped gauges (see Figs. 5 and 11 for more details of the locations of measurement devices).

which reached failure exhibited a crushing of the concrete struts near the loading plate, with the development of a failure surface between the column edge and the first shear reinforcement perimeter. Although the potential failure modes of shear-reinforced specimens are well established, the phenomena that trigger the failure of footings without shear reinforcement is still an object of discussion. In that respect, the continuous measurements recorded in the shear-critical region (near the column) in this experimental campaign provide valuable additional information.

The main deformations measured in the shear-critical region are presented in Fig. 13. Five different measurements are presented: rotation measured near the edges of the footing ψ, column penetration δ_p, changes in the thickness of the specimen measured at a distance of 100 mm from the edge of the steel column plate Δh and the radial $\varepsilon_{c,radial}$ and tangential $\varepsilon_{c,tan}$ strains at the top

concrete surface, both measured at a distance of 100 mm from the edge of the steel column plate. The results presented in Fig. 13 correspond to a) specimen PS11 and b) specimen PS13, which are the most slender and the most compact specimens without shear reinforcement respectively. It is important to note that in both diagrams the load is normalized by the maximum load. With respect to the results, four different regimes of behaviour can be distinguished:

1) Up to ~30 % Q/Q_R, an elastic behaviour can be observed. This led to an increase in rotation (uncracked flexural stiffness), an increase in tangential compression (negative tangential strains) proportional to the rotation, an increase in the radial tension (as a result of local shear deformation near the column, see Fig. 9) and an increase in the support penetration (probably partly due to crushing of the plaster between steel col-
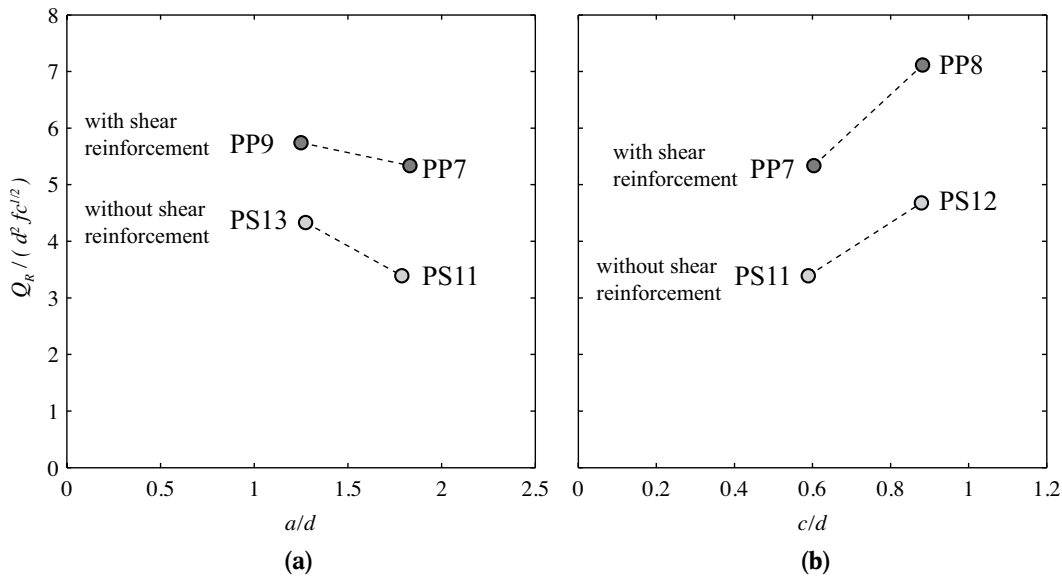
Fig. 14. Normalized load-carrying capacity as a function of a) span-to-effective depth ratio and b) column size-to-effective depth ratio

umn plate and footing). No changes in the thickness of the specimens were observed.

2) From ~30 to ~80 % Q/Q_R for PS11 and ~30 to ~75 % Q/Q_R for PS13, flexural cracks start developing (this was confirmed after visual inspection of the bottom surfaces after testing, see, for instance, Fig. 6) and a decrease in the flexural stiffness can be observed in the load–rotation curve. The tangential compression strains at the concrete top surface increase in proportion to the rotation. The radial tension at the top concrete surface is still increasing as a consequence of a local shear deformation near the column and the penetration of the column accelerates slightly. In the transition between this and the following stage, changes in the thickness of the footing were measured, which may be justified by the appearance of inclined cracks due to the flexural-shear interaction.

3) From ~80 to ~90 % Q/Q_R for PS11 and from ~75 to ~85 % for PS13, the rotation and the column penetration increase, but the corresponding stiffnesses are still approximately equal to the previous regime. The tangential compression at the concrete top surface is still increasing. However, a different behaviour may be observed: the changes in the thickness become important and the radial tension measured at the concrete top surface attains its maximum, remaining approximately constant.

4) Finally, from ~90 % Q/Q_R (PS11) or ~85 % Q/Q_R (PS13) up to maximum load, a slight loss of flexural stiffness (also observed to occur in Fig. 8) is observed, accompanied by a pronounced loss of shear stiffness. The tangential compression at the concrete top surface near the column remains constant or even decreases (decompression). The radial tension at the concrete top surface decreases almost down to zero and the changes in the thickness of the footing and the column penetration accelerate and become very significant.

The four regimes described above were clearly observed for the four footings without shear reinforcement. The limits of each regime depend, however, on the mechanical and geometrical properties. For instance, regime (4) appears to be more significant for more compact footings. This stage might be assumed to correspond to crushing of the concrete struts near the column, which can be confirmed by the signs of crushing observed along the saw-cuts (see Fig. 7). Crushing of the concrete struts near the column would also explain the tangential decompression observed at the concrete top surface (as a consequence of the pronounced lateral expansion of the concrete close to failure [24]). At this stage, the column is penetrating into the footing and the sliding surface forming at the top of the concrete struts is confirmed by the measurements of the changes in thickness (see Fig. 11).

It is also interesting to note that the experimental evidence collected in the campaign presented in this paper are in accordance with those presented by *Hallgren* and *Bjerke* [25], who also observed similar regimes when analysing the punching behaviour of footings using nonlinear finite element analyses.

4 Analysis of experimental evidence
4.1 Influence of span-to-depth ratio and column size

The span-to-depth ratio depends on the footing and column sizes as well as the effective depth. Whereas the nominal value of the latter parameter was kept constant in the experimental investigation presented here, the first two were varied. The maximum loads normalized by the square of the effective depth and the square root of the cylinder concrete compressive strength are presented in Table 2 and shown graphically in Fig. 14 as a function of shear slenderness (equal column size) and column size (for equal side length of footings).The results show that an increase in the shear slenderness reduces the load-carrying capacity for the cases of footings without shear reinforcement (see Fig. 14a) due to:

– an increase in the percentage of load outside the failure surface, where the load has to be carried by inclined struts (increase in shear force), and
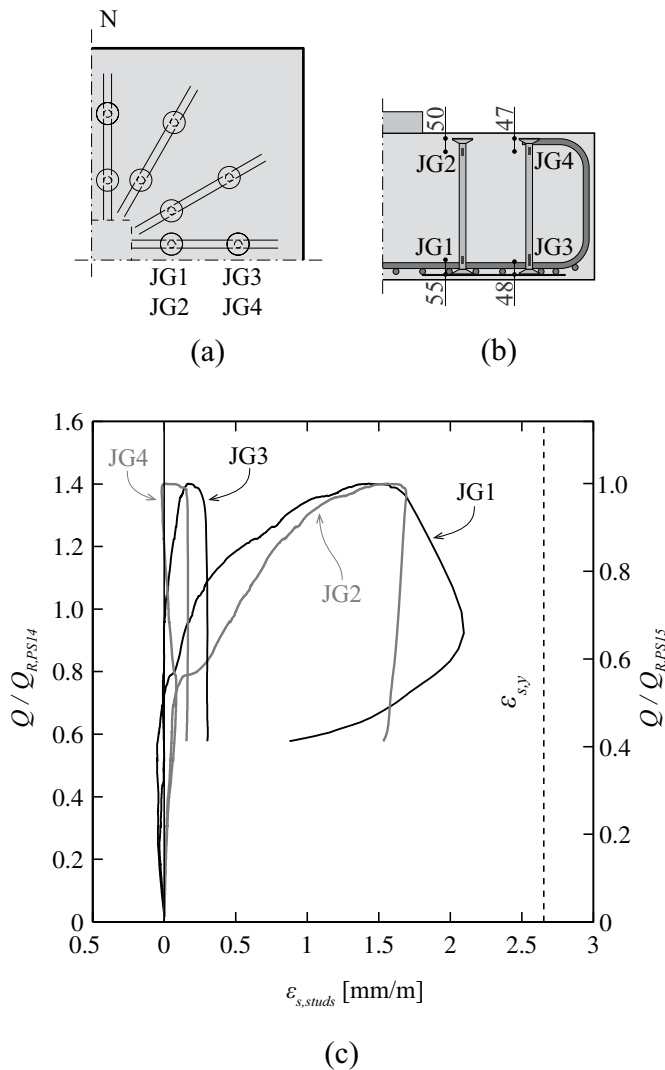
Fig. 15. Strains in shear reinforcement of specimen PS15: a) plan, b) section (showing locations of strain gauges), and c) corresponding load–deformation curves

– a decrease in the inclination of the failure surface (Fig. 7), which is associated with a decrease in the average shear strength per unit length, according to theoretical considerations [26], [27].

As shown in Fig. 14b, increasing the column size leads to an increase in the load-carrying capacity for footings both with and without shear reinforcement. This may be justified not only by the increase in the column perimeter (associated with lower shear stresses acting), but also by the inherent decrease in the shear slenderness (as the side length of the footings was kept constant).

4.2 Influence of shear reinforcement

As was shown previously (see Figs. 8 and 14), the shear reinforcement can enhance the punching strength and deformation capacity compared with specimens without shear reinforcement. Its effectiveness was nevertheless shown to be dependent on the span-to-effective depth ratio, as can be seen in Fig. 14. This has been shown previously for footings having stirrups as shear reinforcement [11]–[14] and is here confirmed for the case of double-headed shear studs. The shear reinforcement

controls the development of transverse strains, as can be seen by comparing the changes in the thickness of footings PS14 and PS15 (see Figs. 11e and 11f) with the activation of the shear reinforcement in footing PS15 (see Fig. 15). The first perimeter of shear studs in specimen PS15 is activated from approx. 80% of the maximum load of the reference specimen PS14, which corresponds to the level of load after which important changes in the thickness of the specimens were measured (Fig. 11). The excellent anchorage conditions of the shear reinforcement used in this experimental campaign (double-headed studs with anchorage head size equal to three diameters) enables its full activation upon the onset of transverse strains.

The decrease in the effectiveness of the shear reinforcement with decreasing shear slenderness may be physically explained by the location and inclination of the concrete struts. Considering that the principal transverse strains develop normal to the compressive strains and that the principal compressive strains have approximately the same direction as the concrete struts, a decrease in the angle between the concrete struts and the shear reinforcement leads to a lower efficiency of the latter [28]. This is the case for footings with a low span-to-effective depth ratio, which have a steeper compression field and, consequently, lower angles between the concrete struts and the shear reinforcement.

4.3 Flexural-shear interaction

It is shown in Fig. 8 that the load–rotation curves of the specimens with shear reinforcement reach a plateau before failure. The strengths at the plateau are significantly lower than those predicted by classical yield line theory [29], [30] and presented in Table 2. This has been shown to occur for slabs with large amounts of shear reinforcement [19], [20]. This phenomenon can be seen as a flexural-shear interaction, as shown using the kinematic theorem of limit analysis [26]. This effect is very important for compact footings [26] since it leads to theoretical values of strength significantly lower than those obtained for a pure flexural failure.

4.4 Influence of top reinforcement

Specimens PS14 and PS15 differ from specimens PS13 and PP9 respectively because horizontal reinforcement was not used in the theoretical compression surface. The objective was to study the potential influence of this reinforcement on the failure mode and strength of the footings. According to theoretical considerations [26], horizontal reinforcement in the compression zone can act as confinement reinforcement for the inclined strut near the column, thus increasing the load capacity. The ratio of the normalized loads (see Table 2) of the specimens with and without horizontal flexural reinforcement confirms that a small increase in the load-carrying capacity can be achieved by including this reinforcement (8% increase for specimens without shear reinforcement, PS13/PS14, and 3% for specimens with shear reinforcement, PP9/PS15).

The expansion of the top and lateral surfaces of specimen PS14 was measured with LVDTs (see Fig. 16a) and the
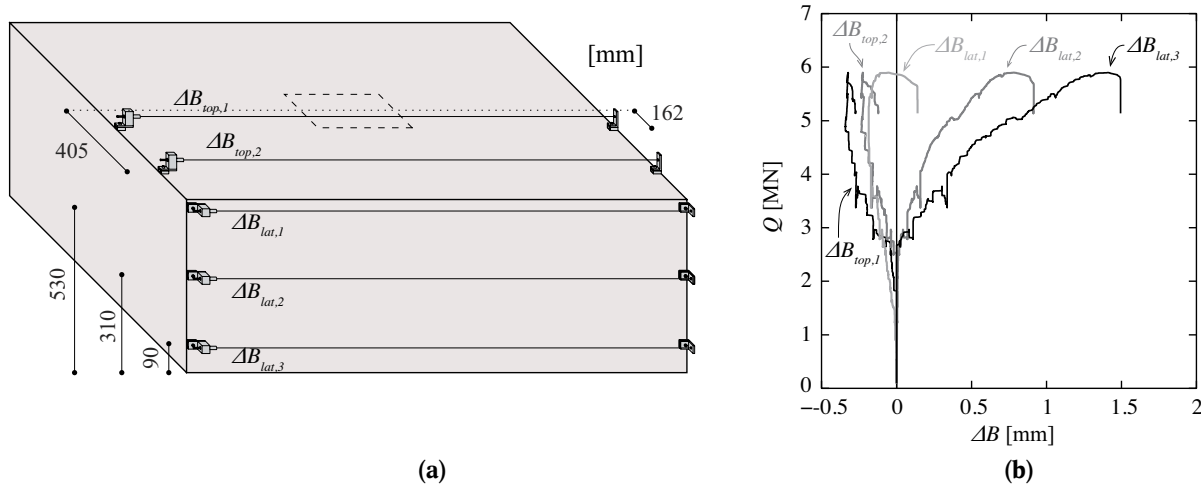
Fig. 16. Changes in width of specimen PS14: a) representation of measurement devices used, b) results (positive values indicate elongation)

results are shown in Fig. 16b. An elongation of the bottom surface (measured at the bottom of the lateral surface) and a shortening of the top surface were measured up to ~80% of the maximum load, probably resulting from the flexural behaviour. After that, although the bottom surface continues to elongate, the shortening of the top surface stabilizes. This may be justified by the expansion of the diagonal concrete strut [24], which compensates for the continuous contraction expected due to the flexural behaviour. Whereas for specimen PS13 (with top flexural reinforcement) no cracks on the top surface could be observed after failure, radial cracks could be seen on the top surface of specimen PS14 (without top reinforcement). Although the expansion of the top surface of specimen PS13 was not measured, the differences in the load-carrying capacity and the crack pattern on the top surface indicate that the presence of top reinforcement might increase the strength of footings without shear reinforcement (this topic should be clarified by future experimental and analytical research).

5 Conclusions

An experimental investigation of eight full-scale reinforced concrete footings with and without shear reinforcement is presented in this paper. The bottom flexural reinforcement (0.75%) and the nominal thickness (550 mm) were kept constant, while the influences of column size, slenderness and the presence of top horizontal reinforcement and shear reinforcement were investigated. Detailed measurements in the shear-critical region were recorded during the experimental tests. The main experimental evidence is summarized in the following:

1) The punching strength of reinforced concrete footings without shear reinforcement is shown to increase with decreasing shear slenderness. Further, the inclination of the critical shear crack appears to be steeper for low span-to-effective depth ratios.
2) The punching strength of reinforced concrete footings can be significantly increased by incorporating double-headed shear studs. The effectiveness of this reinforcement has been shown experimentally to be dependent on the shear slenderness, being less effective for low span-to-effective depth ratios.

3) Although flexural deformations might be important for describing the punching behaviour of footings, significant shear deformations also occur due to the high levels of shear force.
4) A careful analysis of the measurements recorded in the shear critical region indicates that crushing of the concrete diagonal strut close to the column is the phenomenon that triggers failure. Observations of the saw-cuts after testing confirm the presence of crushed concrete in this zone.
5) An important flexural-shear interaction was observed in the case of footings with shear reinforcement, where a plateau appears to be reached in the load–rotation curves.
6) The load corresponding to this flexural-shear plateau is significantly lower than the theoretical flexural capacity calculated based on the yield line method. This reduction may be explained by the high concentrations of shear forces at the edge of the column, which increases the depth of the compression zone and, consequently, decreases the lever arm.
7) The flexural-shear regime described above has to be taken into account in the design and assessment of reinforced concrete footings. A rational-based method to predict the flexural-shear capacity of reinforced concrete footings is needed.

Notation

a/d span-to-depth ratio
B width of specimen
c side length of square column
c/d column size-to-depth ratio
d effective depth
f_c cylinder concrete compressive strength
f_y yield strength of bottom flexural reinforcement

f_{yw} yield strength of shear reinforcement

L distance between LVDTs at edge of footing and near the column

n_s number of studs per perimeter

n_p number of shear reinforcement perimeters

Q load

Q_R maximum load

Q_{flex} flexural capacity

r radius

δ displacement

δ_p column penetration

δ_ψ displacement associated with flexural deformation

δ_γ displacement associated with shear deformation

$\delta_{f,e}$ displacement directly measured at concrete top surface 10 mm from edge of specimen

$\delta_{f,c}$ displacement directly measured at concrete top surface 25 mm from column

δ_c displacement indirectly measured at centre of column plate

ΔB change in side length of specimen

Δh change in thickness of specimen

$\varepsilon_{c,r}$ radial strain at concrete top surface

$\varepsilon_{c,t}$ tangential strain at concrete top surface

$\varepsilon_{s,r}$ radial strain in bottom flexural reinforcement

$\varepsilon_{s,t}$ tangential strain in bottom flexural reinforcement

ρ bottom flexural reinforcement ratio

ϕ_w studdiameter

ψ outer rotation

References

1. *Talbot, A. N.*: Reinforced Concrete Wall Footings and Column Footings, Bulletin 67, Engineering Experiment Station, University of Illinois, 1913.

2. *Richart, F. E.*: Reinforced Concrete Walls and Column Footings, part 1 and 2. ACI Journal, vol. 45, 1948, pp. 97–127& 237–260.

3. *Kordina, K., Nölting, D.*: Load-carrying behaviour of eccentrically loaded isolated reinforced concrete foundations (Tragverhalten von ausmittig beanspruchten Einzelfundamenten aus Stahlbeton), Technical Report, DFG Research 204/27-30, Braunschweig, Germany, 1981 (in German).

4. *Dieterle, H., Rostásy, F.*: Load-carrying behaviour of isolated reinforced concrete foundations of square columns (Tragverhalten quadratischer Einzelfundamente aus Stahlbeton), Deutscher Ausschuss für Stahlbeton, vol. 387, 1987, pp. 1–91 (in German).

5. *Dieterle, H.*: Design of reinforced concrete foundations of square columns under centric loading with the help of design diagrams (Zur Bemessung quadratischer Stützenfundamente aus Stahlbeton unter zentrischer Belastung mit Hilfe von Bemessungsdigrammen), Deutscher Ausschuss für Stahlbeton, vol. 387, 1987, pp. 94–134 (in German).

6. *Hallgren, M., Kinnunen, S., Nylander, B.*: Punching Shear Tests On Column Footings. Nordic Concrete Research, vol. 21, 1998, pp. 1–22.

7. *Timm, M.*: Punching of foundation slabs under axisymmetric loading, Doctoral Thesis, Institute for Building Materials (Durchstanzen von Bodenplatten unter rotationssymmetrischer Belastung), Concrete Structures and Fire Protection of the Technical University Braunschweig, 2003 (in German).

8. *Hegger, J., Sherif, A., Ricker, M.*: Experimental Investigations on Punching Behaviour of Reinforced Concrete Footings. ACI Structural Journal, vol. 103, No. 4, 2006, pp. 604–613.

9. *Ricker, M.*: Punching in RC footings considering the soil-structure-interaction. Proc. of 6th Intl. PhD Symp. in Civil Engineering, Zurich, 2006.

10. *Hegger, J., Ricker, M., Ulke, B., Ziegler, M.*: Investigations on the punching behaviour of reinforced concrete footings. Engineering Structures, vol. 29, No. 9, 2007, pp. 2233–2241.

11. *Hegger, J., Ricker, M., Sherif, A.*: Punching Strength of Reinforced Concrete Footings. ACI Structural Journal, vol. 106, No. 5, 2009, pp. 706–716.

12. *Ricker, M.*: Reliability of punching design of isolated foundations (Zur Zuverlässigkeit der Bemessung gegen Durchstanzen bei Einzelfundamenten). Doctoral thesis, RWTH Aachen University, 2009 (in German).

13. *Siburg, C., Hegger, J.*: Experimental Investigations on Punching Behaviour of Reinforced Concrete Footings with structural dimensions. Structural Concrete, vol. 15, No. 3, 2014, pp. 331–339.

14. *Siburg, C.*: Consistent punching design in flat slabs and foundations (Zur einheitlichen Bemessung gegen Durchstanzen in Flachdecken und Fundamenten). Doctoral thesis, RWTH Aachen University, 2014 (in German).

15. *Netopilik, R. J.*: Punching Shear Behaviour of Thick Reinforced Concrete Slabs. Master thesis, University of Toronto, 2012.

16. *Urban, T., Goldyn, M., Krakowski, J., Krawczyk, L.*: Experimental investigation on punching behaviour of thick reinforced concrete slabs. Archives of Civil Engineering, vol. 59, No. 2, 2013, pp. 157–174.

17. *Krakowski, J., Krawczyk, L., Urban T.*: Punching of RC Thick Plates – Experimental Test and Analysis. Proc. of *fib* Symp., Concrete – Innovation and Design, Copenhagen, 2015.

18. *Urban, T., Krakowski, J., Goldyn, M., Krawczyk, L.*: Punching of RC thick plates, Department of Concrete Structures, Technical University of Lodz, Poland, report No. 19, 2013.

19. *Lips, S.*: Punching of Flat Slabs with Large Amounts of Shear Reinforcement. Thèse EPFL No. 5409, 2012.

20. *Lips, S., Fernández Ruiz, M., Muttoni A.*: Experimental Investigation on Punching Strength and Deformation Capacity of Shear-Reinforced Slabs. ACI Structural Journal, vol. 109, No. 6, 2012, pp. 896–900.

21. *Kinnunen, S., Nylander, H.*: Punching of Concrete Slabs Without Shear Reinforcement. Transactions of the Royal Institute of Technology, No. 158, 1960.

22. *Guandalini, S., Burdet, O., Muttoni, A.*: Punching tests of slabs with low reinforcement ratios. ACI Structural Journal, vol. 106, No. 1, 2009, pp. 87–95.

23. *Fernández Ruiz, M., Muttoni, A.*: Applications of the critical shear crack theory to punching of R/C slabs with transverse reinforcement. ACI Structural Journal, vol. 106 No. 4, 2009, pp. 485–494.

24. *Guidotti, R., Fernández Ruiz, M., Muttoni, A.*: Crushing and Flexural Strength of Slab-Column Joints. Engineering Structures, vol. 33, No. 3, 2011, pp. 855–867.

25. *Hallgren, M., Bjerke, M.*: Non-linear finite element analyses of punching shear failure of column footings. Cement and Concrete Composites, vol. 24, No. 6, 2002, pp. 491–496.

26. *Simões, J. T., Faria, D. V., Fernández Ruiz, M., Muttoni, A.*: Strength of reinforced concrete footings without transverse reinforcement according to limit analysis. Engineering Structures, vol. 112, pp. 146–161.

27. *Braestrup, M. W., Nielsen, M. P., Jensen, B. C., Bach, F.*: Axisymmetric Punching of Plain and Reinforced Concrete, Report No. 75, Structural Research Laboratory, Technical University of Denmark, 1976.

28. *Vecchio, F. J., Collins, M. P.*: The modified compression-field theory for reinforced concrete elements subjected to shear. ACI Journal, vol. 83, No. 2, 1988, pp. 219–231.

29. *Johansen, K.W.*: *Yield-line Theory,* Cement and Concrete Association, 1962.
30. *Gesund, H.*: Flexural Limit Analysis of Concentrically Loaded Column Footings. ACI Journal Proceedings, vol.80, No. 3, 1983, pp. 223–228.

João T. Simões
PhD Candidate
École Polytechnique Fédérale de Lausanne
ENAC, Station 18, CH-1015, Lausanne
Switzerland
joao.simoes@epfl.ch

Jan Bujnak
R&D Manager
Peikko Group
jan.bujnak@peikko.com

Miguel Fernández Ruiz
Lecturer and Senior Scientist
École Polytechnique Fédérale de Lausanne
ENAC, Station 18, CH-1015, Lausanne
Switzerland
miguel.fernandezruiz@epfl.ch

Aurelio Muttoni
Professor
École Polytechnique Fédérale de Lausanne
ENAC, Station 18, CH-1015, Lausanne
Switzerland
aurelio.muttoni@epfl.ch